Letter

ADVANCED PHOTONICS

Observation of robust subwavelength phase singularity in chiral medium

Jun-Hee Park,[a] Jeongho Ha,[a] Liyi Hsu,[a] Guang Yang,[b] Yeshaiahu Fainman,[a] Alexander V. Sergienko,[b] and Abdoulaye Ndao[a,b,*]

[a]University of California, San Diego, Department of Electrical and Computer Engineering, La Jolla, California, United States
[b]Boston University, Photonics Center, Department of Electrical and Computer Engineering, Boston, Massachusetts, United States

Abstract. Photonic devices that exhibit both sensitivity and robustness have long been sought; yet, these characteristics are thought to be mutually exclusive; through sensitivity, a sensor responds to external stimuli, whereas robustness embodies the inherent ability of a device to withstand weathering by these same stimuli. This challenge stems from the inherent contradiction between robustness and sensitivity in wave dynamics, which require the coexistence of noise-immune sensitive states and modulation-sensitive transitions between these states. We report and experimentally demonstrate a subwavelength phase singularity in a chiral medium that is resilient to fabrication imperfections and disorder while remaining highly responsive to external stimuli. The combination of subwavelength light confinement and its robustness lays the foundation for the development of hitherto unexplored chip-scale photonics devices, enabling a simultaneous development of high-sensitivity and robust devices in both quantum and classical realms.

Keywords: plasmonic; resonator; robustness; phase singularity; subwavelength; chirality; metamaterials.

Received Sep. 16, 2024; revised manuscript received Dec. 16, 2024; accepted for publication Feb. 21, 2025; published online Mar. 17, 2025.

[DOI: 10.1117/1.AP.7.3.035001]

1 Introduction

In 1811, Arago reported that linearly polarized light traveling through a quartz crystal experiences a rotation of its plane of polarization.[1] The concept of chirality, however, was not born until 1848, when Pasteur discovered the configurational isomers of asymmetric molecules.[2] Since then, chirality, or handedness of molecules, has continued to fascinate the scientific world and constitutes the bedrock of today's many technological and scientific advancements in physics, chemistry, and life sciences.[3–7] Chirality, an essential attribute of many life systems, manifests in the form of two molecular structural forms known as enantiomers, showcasing its fundamental symmetry property throughout the universe on scales ranging from galaxies to subatomic particles.[8,9] Although two enantiomers, a chiral molecule and its mirror image, share many physical and chemical properties, they can diverge in terms of activation and function. Observing the effects at the molecular level reveals how it can have triumphant or tragic results in various contexts. For example, the drug thalidomide has one enantiomer that effectively relieves morning sickness in pregnant women, whereas the other, tragically, causes severe congenital disabilities.[10–12] Therefore, a robust method that rapidly identifies enantiomers and assesses their purity is urgently needed. Enantioselectivity technologies using light are usually based on nondestructive probing of the system in question with electromagnetic waves, typically utilizing enhanced wave–matter interaction at resonances.

To date, observations of chiral photonic devices have been limited to intensity-based settings that either have a low spectral resolution because of the high levels of scattering and dissipation losses or are diffraction-limited, as well as sensitive to fabrication imperfections.[13–30] Furthermore, conventional light sources used in intensity-based measurement suffer from high-intensity (amplitude) noise, thus reducing the detection sensitivity of intensity-based settings.[29]

By contrast, as a fundamental property of light characterized by its sensitivity to phase singularity, it gives rise to a myriad of intriguing features of phase behaviors including the Berry phase

*Address all correspondence to Abdoulaye Ndao, a1ndao@ucsd.edu

of quantum systems, the Pancharatnam phase of light, vortex beams, and Heaviside step-like jumps.[31–33]

Such Heaviside step-like phase jumps possess a singularity whereby the light intensity crosses zero, whereas the phase around the singularity proceeds continuously through all phase values ranging from 0 to 2π. Contours of such points of darkness form a continuous line in a multi-dimensional space, but an individual singular point can be found in a given two-dimensional parameter space if such a plane intersects with the contour line.

Achieving photonic devices that combine sensitivity and robustness has been a longstanding challenge in optics, as these characteristics are often viewed as fundamentally incompatible. Sensitivity enables a device to respond to external stimuli, whereas robustness ensures stability against disturbances, creating an apparent paradox in wave dynamics. This paradox arises from the conflicting requirements: robust operation demands noise-immune stable states, whereas sensitivity necessitates transitions responsive to external modulations. In this work, we resolve this contradiction by introducing a phase singularity inherently resilient to fabrication imperfections and disorder, ensuring robustness while maintaining high sensitivity to external stimuli. The increasing interest in generating and manipulating phase singularities stems from their sensitivity, portraying them as ideal platforms for applications such as optical communications, imaging, and sensing systems.[34–41] Moreover, with the proper design of a sensor scheme, phase noise can be orders of magnitude lower than those belonging to amplitudes [typically ranging from 10^{-6} to 10^{-5} refractive index units (RIU)], resulting in a significantly higher signal-to-noise ratio (10^{-8} RIU).[42,43] Despite its significant advantages, using robust phase-based sensing in chiral media presents an untapped frontier that holds promising potential for advancing sensing in classical and quantum realms.

Here, we report for the first time a subwavelength phase singularity in a chiral medium that is resilient to fabrication imperfections and disorder while remaining highly responsive to external stimuli.

2 Principles and Methods

To demonstrate the phase singularity in a chiral medium, the structure is implemented in a bilayer array of subwavelength plasmonic resonators with twisted angle θ. The bilayer nanostructure comprises two plasmonic nanorod arrays interleaved by a subwavelength-thick polymer spacer (SU-8). The bottom layer of resonators is embedded in SU-8, whereas the top array layer of resonators is exposed to the air, making its surface available for chiral analyte detection. The two different polarizations of light [right-handed circularly polarized (RCP), in red, and left-handed circularly polarized (LCP), in blue] are incident onto the front side of the bilayer and transmitted to the backside (substrate) [Fig. 1(a)].

Figure 1(b) illustrates the unit cell geometry with their design parameters. Each unit cell consists of spatially separated plasmonic nanorods, which are twisted at angles ($\theta = 30$ deg) with respect to one another. The two layers of nanorods are displaced by d_x in the X-direction as an engineered degree of freedom. L_{top} represents the length of the top bars, whereas L_{bottom} represents the length of the bottom bars. The bilayer nanostructures are fabricated using two-step electron beam lithography (EBL) and metal lift-off on a glass substrate (refractive index $n_{\text{sub}} = 1.50$). First, the metal array patterns were defined in the bilayer electron beam resists, followed by metal deposition and a lift-off process. Then, a 60-nm-thick SU-8 (h_s) is spun over on the first metal array as a planarized dielectric layer ($n_{\text{SU-8}} = 1.57$). Finally, the second layer was fabricated using the same method but included a precise alignment process (see Fig. S2 and Fig. S3 in the Supplementary Material). Figure 1(c) presents an enlarged top-view SEM image of the fabricated multilayer structure, with a lateral shift between nanorods $d_x = 80$ nm and a twisted angle ($\theta = 30$ deg), demonstrating excellent alignment accuracy between the two functional layers and uniform surface texture and morphology (see Fig. S4 in the Supplementary Material). Although the oblique incidence of light is typically utilized in the design of phase singularities, our proposed platform operates under normal incidence, thus simplifying the sensing mechanism and its integration process into a single chip. To achieve the point of darkness (phase singularity), we sweep only one geometrical parameter, the lateral displacement d_x, which controls the coupling between two resonators.

To investigate the optical response of the device to a circularly polarized light illumination, full-wave electromagnetic

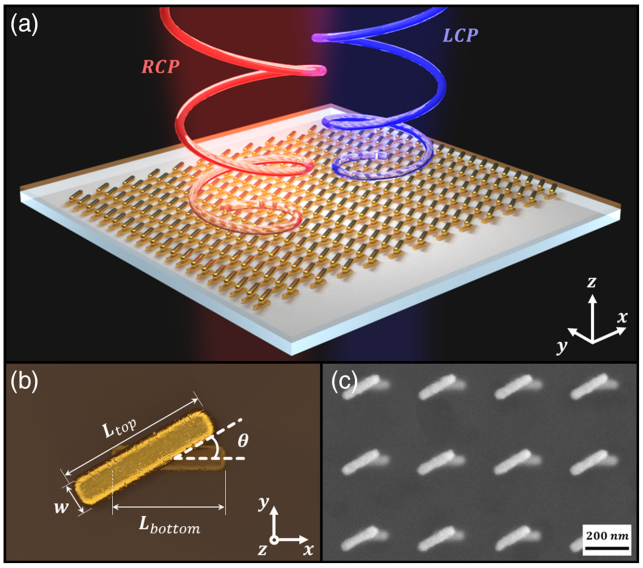

Fig. 1 Multilayered periodic photonic nanostructure supporting robust phase singularity. (a) Schematic of the periodic bilayer structure enabling robust phase singularity; the array is made of two plasmonic resonators with detuned resonances and twisted angle θ. The first layer of resonators is embedded in a 60-nm-thick polymer spacer (SU-8), whereas the second layer of resonators is on top of the polymer and is exposed to the air, making its surface available for chiral analyte detection. Panel (b) illustrates the unit cell consisting of two spatially separated plasmonic nanorods twisted at an angle ($\theta = 30$ deg). L_{top} represents the lengths of top bars while L_{bottom} represents the length of the bottom bars. The structures are fabricated using two-step electron beam lithography (EBL) and metal lift-off on a glass substrate ($n_{\text{sub}} = 1.50$). Finally, the second layer was fabricated using the same method but included a precise alignment process. (c) Top-view scanning electron microscope (SEM) image of the fabricated multilayer structure, with $d_x = 80$ nm and twisted angle $\theta = 30$ deg, showing the quality of the fabricated structures.

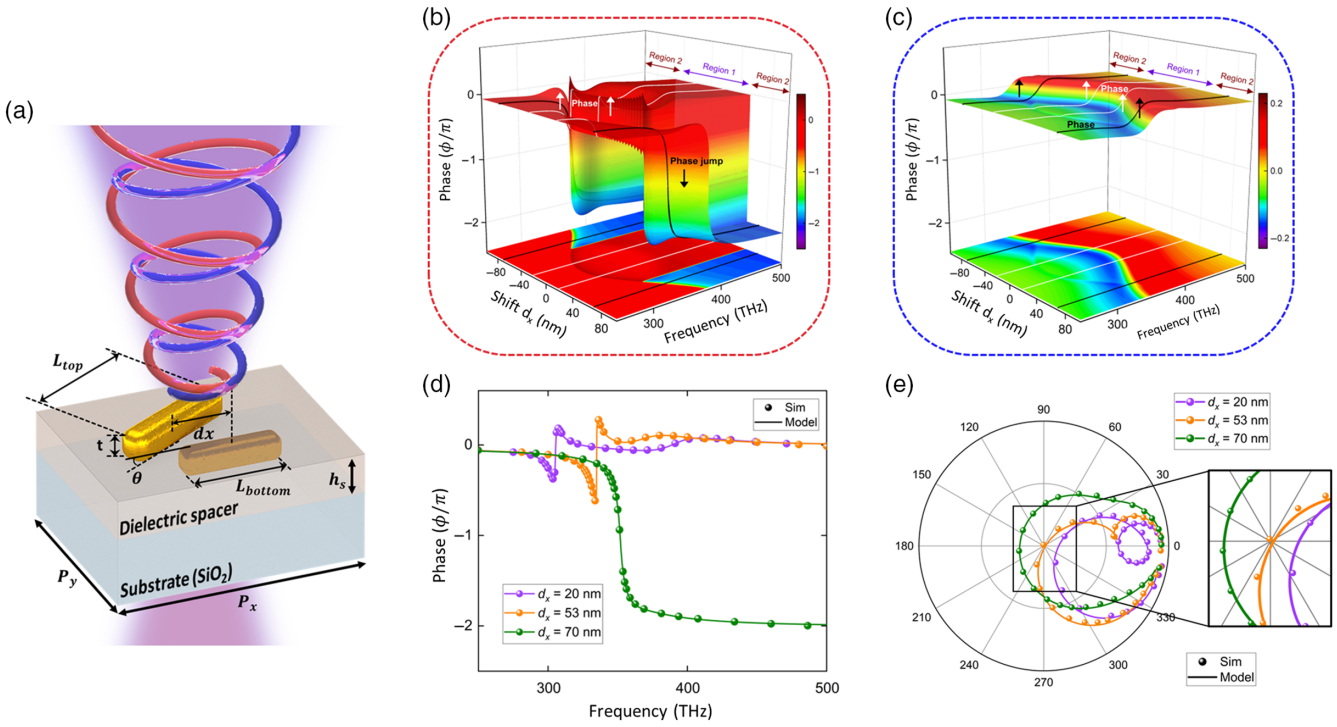

Fig. 2 Hybridized plasmonic arrays of spatially separated plasmonic twisted resonators with two different incident beams (RCP and LCP). (a) Schematic of a bilayer unit cell structure made of two plasmonic resonators in an array with twisted resonators at a twisted angle ($\theta = 30$ deg). RCP light (red color) and LCP light (blue color) are incident onto the front side of the bilayer plasmonic nanostructure, and transmitted through the substrate. The unit cell dimensions consist of dissimilar gold nanorods with different parameters $L_{\text{top}} = 170$ nm, $L_{\text{bottom}} = 120$ nm, $W = 50$ nm, and $t = 40$ nm. The phase response is designed using the same configuration with two different incident beams RCP and LCP. (b) Numerical simulation shows the existence of phase singularity when incident light is RCP, thus highlighting the phase singularity in a chiral medium (red box). The phase singularity occurs around $d_x = 53$ nm. Panel (c) represents a regular phase when illuminated by a left circularly polarized light (blue box). Panel (d) represents the comparison between the numerical simulation and the developed model (see Supplementary Material). (e) The polar plot illustrates the complex amplitudes of the transmission. In this chart, the dots represent the numerical simulation, whereas solid lines depict the fits obtained through the model (with polar angles in deg).

simulations were first performed using computer simulation technology (CST). Figure 2 presents the numerical simulations of the phase response of the hybridized plasmonic arrays using incident beams (RCP, in red; LCP, in blue).

Figure 2(a) represents the unit cell of the proposed configuration. LCP light (blue) and RCP light (red) are incident onto the front side of the bilayer plasmonic nanostructure and transmitted through the substrate. By varying the offset d_x, the coupling of the two metal bars is tuned, and regular phase response and phase singularity can be observed when the structure is illuminated, with two different circular polarizations of the incident light. Thus, the designed chiral nanostructure exhibits a strong phase behavior with the light with a particular handedness while maintaining a regular phase behavior with another one. The two layers of nanorods are displaced by d_x in the X-direction. The gold nanorods have a length of $L_{\text{top}} = 170$ nm, $L_{\text{bottom}} = 120$ nm, a width of $W = 50$ nm, a periodicity of $P_x = P_y = 350$ nm, and a thickness of $t = 40$ nm. Figure 2(b) shows the existence of phase singularity for right circularly polarized light, thus highlighting the phase singularity in chiral medium. The phase singularity occurs around $d_x = 53$ nm.

On the other hand, Fig. 2(c) represents a regular phase when a left circularly polarized light illuminates the structure. It is worth noting theoretically, switching from RCP light to LCP light within the same optical configuration (e.g., at a twist angle of $\theta = 30$ deg) is fundamentally equivalent to using two configurations with opposite angular orientations (e.g., $\theta = 30$ deg and $\theta = -30$ deg) while keeping the incident light conditions (LCP or RCP) unchanged. This symmetry arises because the change in polarization handedness reverses the interaction between the light and the system, producing the same effect as flipping the twisted angle (see Fig. S7 in the Supplementary Material).

To comprehend the origin of the robustness, we use a coupled mode theory (CMT) to model it. First, we considered the simplest case, which consists of a single-mode optical resonator coupled with one port (see Sec. 1 in the Supplementary Material). Then, we extended it to two modes with two ports.

By time-reversal symmetry and considering two loss mechanisms, radiation (Γ_r) and absorption loss (Γ_a), the reflection coefficient r can be written as

$$r = \frac{2\Gamma_r}{-i(\omega-\omega_0)+\Gamma_r+\Gamma_a} + \beta_1, \tag{1}$$

ω is the frequency and ω_0 is the resonance frequency of the resonator. β_1 is a proportionality constant. Then, we extended it to two modes with two ports, and the transmission coefficient t can be expressed as

$$t = t_0 e^{i\Phi_0} + \frac{\Gamma_{1r} e^{i\Phi_1}}{i(\omega-\omega_1)-\Gamma_{1r}-\Gamma_{1a}} + \frac{\Gamma_{2r} e^{i\Phi_2}}{i(\omega-\omega_2)-\Gamma_{2r}-\Gamma_{2a}}. \tag{2}$$

The first term corresponds to the complex transmission without the resonators (due to the background medium). The second and the third terms are the ones with the first and the second resonators with resonance frequency ω_1 and ω_2. Γ is the loss rate of the resonance; subscripts r and a indicate radiation loss and absorption loss, respectively. t_0 and Φ_0 are the amplitude and the phase part of the transmission term for the background medium. Φ_1 and Φ_2 are the phase parts for the first and the second resonators.

Details of the model and more numerical simulations are presented in the Supplementary Material. Figure 2(d) shows a very good agreement between numerical simulations (solid line) and the CMT (dots), illustrating additional proof of the existence of the phase singularity in the chiral medium.

In Fig. 2(e), the polar plot shows the complex amplitude of the transmission. In this plot, the dots represent the numerical simulation, whereas solid lines depict the best fit obtained through the model; $d_x = 20$ nm (purple color) and $d_x = 70$ nm (green color) represent, respectively, the under-coupling and over-coupling regime, whereas $d_x = 53$ nm represents the critical coupling (orange color) corresponding to zero transmission, thus indicating the point of darkness.

3 Experiment Results

To experimentally demonstrate the existence of the robust phase singularity in a chiral medium, we characterize the structures of Fig. 1 using two different circularly polarized lights (RCP and LCP) (see Fig. S5 in the Supplementary Material). Figure 3 presents experimental (circles) and simulated phase results (lines). A very good agreement is obtained between numerical simulations and experiments. Dimensions are chosen to support a phase jump ($L_{\text{top}} = 170$ nm, $L_{\text{bottom}} = 120$ nm, $W = 50$ nm, $\theta = 30$ deg). By varying the offset d_x as a function of the frequency, the phase jump occurs at zero transmission (see Supplementary Material). The phase singularity occurs between $d_x = 48$ and 58 nm. Error bars indicate the standard deviation of measured phases. We observe a phase jump at $d_x = 58$ nm and a regular phase at $d_x = 48$ nm under RCP incidence, whereas they maintain regular phase behavior under LCP incidence. This shows unambiguously the existence of phase singularity. The experimental results are obtained by measuring the phase of the transmitted light. It is worth noting that measuring the singularities cannot be achieved directly through darkness due to the absence of light and extreme phase jumps. Therefore, working in the vicinity of the point of darkness is necessary. For instance, this can be easily accomplished by slightly adjusting the geometrical parameters (offset d_x). The transmitted phase is measured using a custom interferometer (see Supplementary Material), whereas the transmittance is measured using a Fourier-transform infrared spectrometer (Bruker Vertex 70) combined with an infrared microscope. For extracting the transmission phase of the device, our

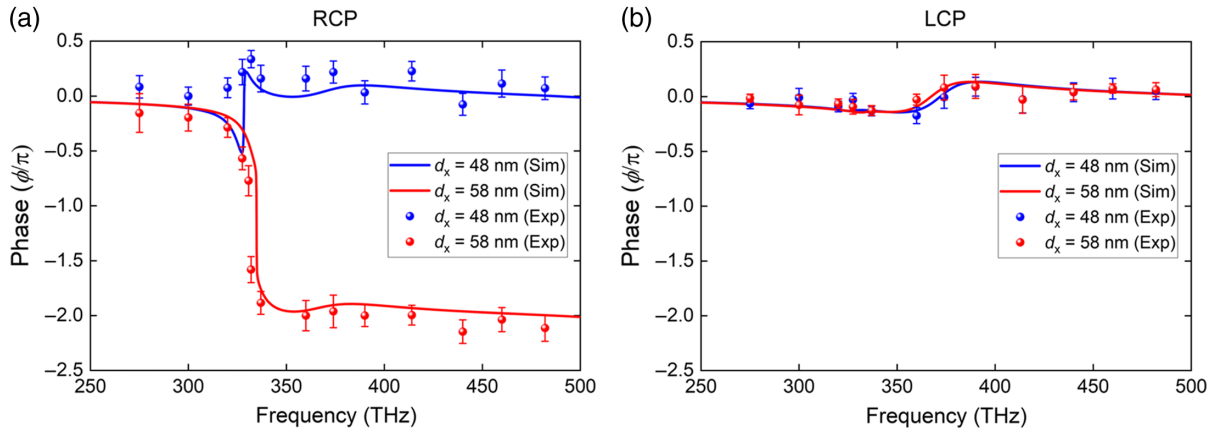

Fig. 3 Experimental observation of phase singularity in a chiral medium. Panels (a) and (b) present the comparison between numerical simulations and experimental phase responses of the hybridized plasmonic arrays of two spatially separated plasmonic twisted resonators at a twisted angle ($\theta = 30$ deg) with RCP (a) and LCP (b) as the incident beams. Dimensions are chosen to support a phase jump ($d_x = 58$ nm, $L_{\text{top}} = 170$ nm, $L_{\text{bottom}} = 120$ nm, $W = 50$ nm, $\theta = 30$ deg). Left and right circularly polarized lights are incident onto the front side of the bilayer plasmonic nanostructure and transmitted through the substrate. By varying the offset d_x as a function of the frequency, the phase jump occurs at zero transmission (see Supplementary Material). The phase singularity occurs between $d_x = 48$ and 58 nm. Error bars indicate the standard deviation of measured phases.

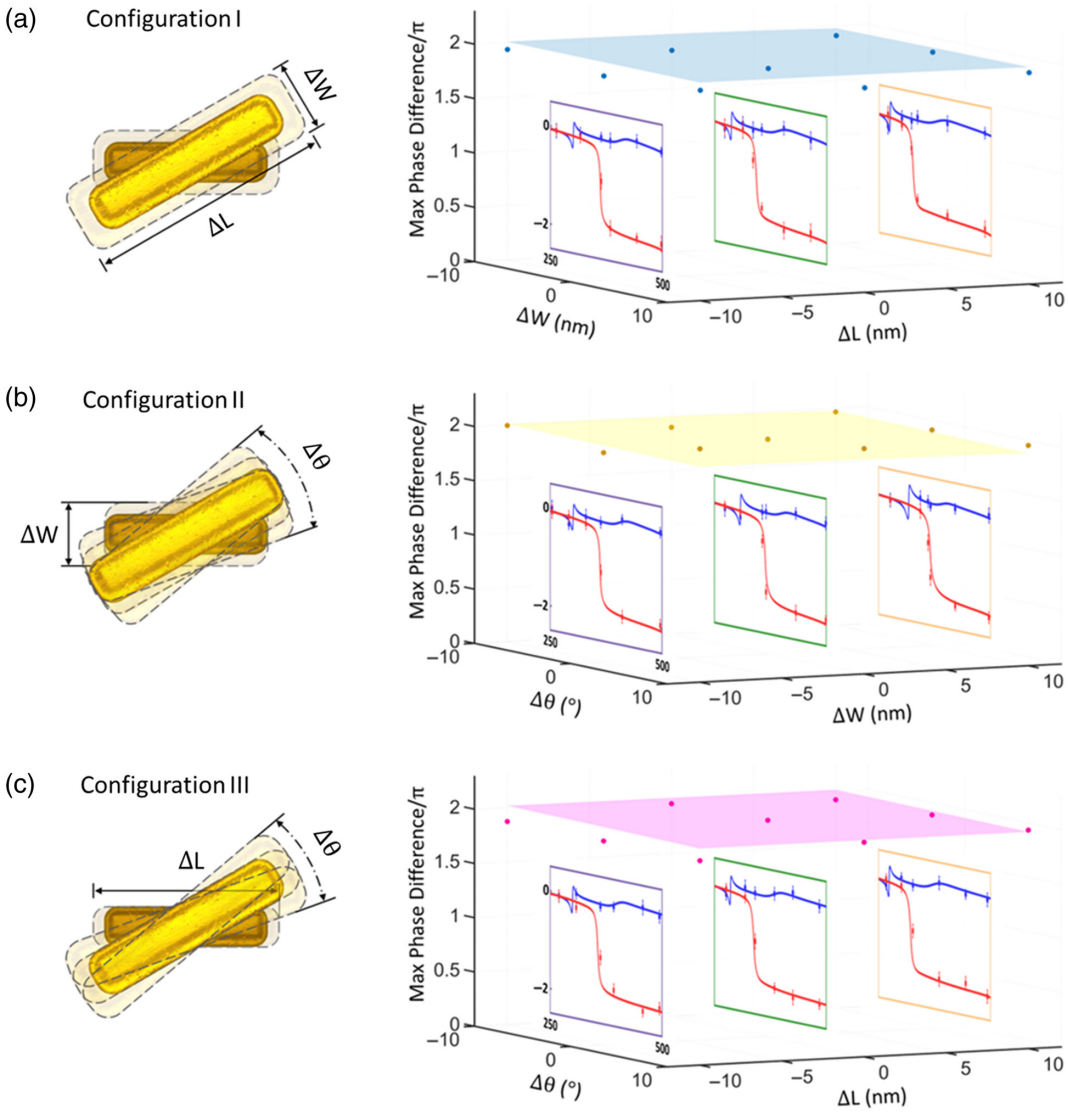

Fig. 4 Robustness of phase singularity in a chiral medium using three primary parameters, width (W), length (L), and twisted angle (θ), as well as the effects of various combinations of these parameters on the performance of the devices. The sweeping ranges are width from 50 to 70 nm ($\Delta W = -10$ to 10 nm, $W_{\text{center}} = 60$ nm), length from 170 to 190 nm ($\Delta L = -10$ to 10 nm, $L_{\text{center}} = 180$ nm), and twisted angle from 30 deg to 50 deg ($\Delta\theta = -10$ deg to 10 deg, $\theta_{\text{center}} = 40$ deg). Panel (a) represents configuration I where $\theta = 30$ deg with varying L and W. Panel (b) represents configuration II where $L = 170$ nm with varying θ and W. Panel (c) illustrates configuration III where $W = 50$ nm with varying L and W. The insets are 2D plots including regular phase ($d_x = 0$ nm, blue) and phase jump ($d_x = 80$ nm, red) such as in Fig. 3(a). The insets in panel (a) are the case of $\Delta W = 0$ nm with $\Delta L = -10$, 0, and 10 nm. The insets in panel (b) are the case of $\Delta\theta = 0$ deg with $\Delta W = -10$, 0, and 10 nm. The insets in panel (c) are the case of $\Delta\theta = 0$ deg with $\Delta L = -10$, 0, and 10 nm. The lines are simulations, and dots/squares are experimental data with an error bar. The error bar indicates the standard deviation of measured phases. A max phase difference is calculated by subtracting the phase of the regular case from the phase jump case at the highest frequency. When a phase singularity exists in the system, the max phase difference is close to 2π. We can observe the max phase difference/π in the 3D plots of different sweeping variables in Fig. 4 are all close to 2 (surfaces are simulations, and dots are measurements). Thus, the proposed photonic device is robust, as fabrication imperfections cannot hinder the existence of phase singularities.

experimental system comprises a wavelength-tunable source, a dispersion-canceling free-space Mach-Zehnder interferometer (MZI), and a post-processing scheme based on fast Fourier transform to extract the phase response from interferograms captured by a camera. The experimentally measured optical transmission of both the RCP and LCP agreed well with the numerical simulations (see Fig. S6 in the Supplementary Material).

A key approach to quantifying the robustness of photonic devices involves intentionally modifying physical parameters to replicate the real-world imperfections resulting from the fabrication process, thereby defining the inherent limitations of optical sensors. To assess the robustness of the phase singularity, we examine the response of our plasmonic devices with respect to three primary parameters—width (W), length (L), and twist angle (θ)—as well as the effects of various combinations of these three parameters on the performance of the devices. To compute that, various unit cells of periodic nanostructures have been experimentally employed to observe the robustness of the singularities (Fig. 4). The sweeping ranges are width from 50 to 70 nm ($\Delta W = -10$ to 10 nm, $W_{\text{center}} = 60$ nm), length from 170 to 190 nm ($\Delta L = -10$ to 10 nm, $L_{\text{center}} = 180$ nm), and twisted angle from 30 deg to 50 deg ($\Delta\theta = -10$ deg to 10 deg, $\theta_{\text{center}} = 40$ deg). Figure 4(a) represents a configuration of $\theta = 30$ deg with varying L and W. The insets are 2D plots including regular phase ($d_x = 0$ nm, blue) and phase jump ($d_x = 80$ nm, red). The insets in Fig. 4(a) are the case of $\Delta W = 0$ nm with $\Delta L = -10$, 0, and 10 nm. Figure 4(b) represents the case where $L = 170$ nm with varying θ and W. The insets in Fig. 4(b) are the case where $\Delta\theta = 0$ deg with $\Delta W = -10$, 0, and 10 nm. Figure 4(c) illustrates the case where $W = 50$ nm with varying L and W. The insets in Fig. 4(c) are the case where $\Delta\theta = 0$ deg with $\Delta L = -10$, 0, and 10 nm. The lines are simulations, and dots/squares are experimental data with an error bar. The error bar indicates the standard deviation of the measured phases. A max phase difference is calculated by subtracting the phase of the regular case from the phase jump case at the highest frequency (for more details, see Table 1 in the Supplementary Material). When a phase singularity exists in the system, the max phase difference is close to 2π. We can observe the max phase difference/π in the 3D plots for different sweeping variables in Fig. 4 is close to 2 for all (surfaces are simulations, and dots are measurements). Thus, the proposed photonic device is robust, as fabrication imperfections cannot hinder the existence of phase singularities. This is in contrast with design-based machine learning, which is often difficult to fabricate and computationally heavy.[44,45]

Calculating the phase enables us to show the robustness of the chiral sensors. Our proposed approach is more robust than standard conventional optical sensors. This progress represents a major leap forward in engineering photonic devices by harnessing the robustness and unique properties of non-Hermitian systems. It has the potential to develop highly sensitive sensors and efficient signal amplifiers in both classical and quantum realms, thereby significantly expanding our toolkit for new technology in unprecedented and transformative ways.

4 Conclusion

We have reported the first experimental demonstration of subwavelength robust phase singularities in a chiral medium. Phase singularity exhibits significant potential for practical applications, as it can alleviate the strict constraints imposed by fabrication tolerances. This property enables more flexible design and fabrication of devices that utilize phase singularities, which can be challenging to achieve with conventional methods. The groundbreaking combination of subwavelength light confinement and robustness phase singularities lays the foundation for hitherto unexplored chip-scale photonics devices, enabling the development of high-sensitivity devices in both quantum and classical realms.

Disclosures

No conflicts of interest, financial or otherwise, are declared by the authors.

Code and Data Availability

The computer codes and the data that support the plots within this paper and other findings of this study are available from the corresponding author upon reasonable request.

Acknowledgments

This work was supported by the 2023 Beckman Young Investigator Award, from the Arnold and Mabel Beckman Foundation; Air Force Office of Scientific Research MURI (Award No. FA9550-22-1-0312); PAIR-UP program sponsored by ASCB, and funded in part by The Gordon Moore Foundation, with additional support from the Burroughs Wellcome Funds; 2022 Scialog: Advancing BioImaging; Kavli Innovation Grant; Silicon Valley Community Foundation (Grant No. DAF2023-331948); cZi Dynamic imaging via the Chan Zuckerberg Donor Advised Fund (DAF) through the Silicon Valley Community Foundation.

References

1. D. F. G. Arago, *Mémoire sur une modification remarquable qu' éprouvent les rayons lumineux dans leur passage à travers certains corps diaphanes, & sur quelques autres phénomènes d'optique*, [Memoir on a remarkable modification experienced by light rays in their passage through certain diaphanous bodies and on some other optical phenomena], Institut national de France [French National Institute], Paris (1811).
2. L. Pasteur, *Recherches sur les relations qui peuvent exister entre la forme cristalline, la composition chimique et le sens de la polarisation rotatoire* [Research on the relations that may exist between the crystalline form, the chemical composition and the directions of rotational polarization], Bachelier, Paris (1848).
3. W. T. B. Kelvin, *Baltimore Lectures on Molecular Dynamics and the Wave Theory of Light*, C.J. Clay and Sons (1904).
4. E. Hendry et al., "Ultrasensitive detection and characterization of biomolecules using superchiral fields," *Nat. Nanotech.* **5**(11), 783–787 (2010).
5. R. Tullius, A. S. Karimullah, and M. Rodier, "Superchiral spectroscopy: detection of protein higher order hierarchical structure with chiral plasmonic nanostructures," *J. Am. Chem. Soc.* **137**(26), 8380–8383 (2015).
6. D. Schamel et al., "Chiral colloidal molecules and observation of the propeller effect," *J. Am. Chem. Soc.* **135**(33), 12353–12359 (2013).
7. C. Wagenknecht et al., "Experimental demonstration of a heralded entanglement source," *Nat. Photon.* **4**(8), 549–552 (2010).
8. M. M. Green and J. V. Selinger, "Cosmic chirality," *Science* **282**(5390), 879 (1998).
9. W. Ma et al., "Chiral inorganic nanostructures," *Chem. Rev.* **117**(12), 8041–8093 (2017).
10. J. F. Sherson et al., "Quantum teleportation between light and matter," *Nature* **443**(7111), 557–560 (2006).

11. W. G. McBride, "Thalidomide and congenital abnormalities," *The Lancet* **278**, 1358 (1961).
12. J. McCredie and W. G. McBride, "Some congenital abnormalities: possibly due to embryonic peripheral neuropathy," *Clin. Radiol.* **24**(2), 204–211 (1973).
13. Y. Chen et al., "Observation of intrinsic chiral bound states in the continuum," *Nature* **613**(7944), 474–478 (2023).
14. P. Kumar et al., "Photonically active bowtie nanoassemblies with chirality continuum," *Nature* **615**(7952), 418–424 (2023).
15. T. Shi et al., "Planar chiral metasurfaces with maximal and tunable chiroptical response driven by bound states in the continuum," *Nat. Commun.* **13**(1), 4111 (2022).
16. R. M. Kim et al., "Enantioselective sensing by collective circular dichroism," *Nature* **612**(7940), 470–476 (2022).
17. A. Qu et al., "Stimulation of neural stem cell differentiation by circularly polarized light transduced by chiral nanoassemblies," *Nat. Biomed. Eng.* **5**(1), 103–113 (2021).
18. B. Semnani et al., "Spin-preserving chiral photonic crystal mirror," *Light Sci. Appl.* **9**(1), 23 (2020).
19. Q. Zhang et al., "Unraveling the origin of chirality from plasmonic nanoparticle-protein complexes," *Science* **365**(6460), 1475–1478 (2019).
20. Z. Wu et al., "High-performance ultrathin active chiral metamaterials," *ACS Nano* **12**(5), 5030–5041 (2018).
21. M. Hentschel et al., "Chiral plasmonics," *Sci. Adv.* **3**(5), e1602735 (2017).
22. S. Zhang, J. Zhou, and Y. S. Park, "Photoinduced handedness switching in terahertz chiral metamolecules," *Nat. Commun.* **3**(1), 942 (2012).
23. A. Y. Zhu et al., "Giant intrinsic chiro-optical activity in planar dielectric nanostructures," *Light Sci. Appl.* **7**(2), 17158 (2018).
24. Y. Zhao et al., "Chirality detection of enantiomers using twisted optical metamaterials," *Nat. Commun.* **8**(1), 14180 (2017).
25. C. Wu et al., "Spectrally selective chiral silicon metasurfaces based on infrared Fano resonances," *Nat. Commun.* **5**(1), 3892 (2014).
26. Y. Cui et al., "Giant chiral optical response from a twisted-arc metamaterial," *Nano Lett.* **14**(2), 1021–1025 (2014).
27. W. Li et al., "Circularly polarized light detection with hot electrons in chiral plasmonic metamaterials," *Nat. Commun.* **6**(1), 8379 (2015).
28. V. K. Valev et al., "Chirality and chiroptical effects in plasmonic nanostructures: fundamentals, recent progress, and outlook," *Adv. Mater.* **25**(18), 2517–2534 (2013).
29. A. V. Kabashin et al., "Plasmonic nanorod metamaterials for biosensing," *Nat. Mater.* **8**(11), 867–871 (2009).
30. Z. Li et al., "Spin-selective full-dimensional manipulation of optical waves with chiral mirror," *Adv. Mater.* **32**(26), 1907983 (2020).
31. Y. H. Huang et al., "Phase-sensitive surface plasmon resonance biosensors: methodology, instrumentation and applications," *Ann. Phys.* **524**(11), 637–662 (2012).
32. M. Berry, "Making waves in physics," *Nature* **403**(6765), 21 (2000).
33. J. F. Nye and J. V. Hajnal, "The wave structure of monochromatic electromagnetic radiation," *Proc. R. Soc. Lond. A* **409**, 21–36 (1997).
34. F. Ding et al., "Electrically tunable topological phase transition in non-Hermitian optical MEMS metasurfaces," *Sci. Adv.* **10**(5), eadl4661 (2024).
35. K. O'Holleran, M. R. Dennis, and M. J. Padgett, "Topology of light's darkness," *Phys. Rev. Lett.* **102**(14), 143902 (2009).
36. A. N. Grigorenko, P. I. Nikitin, and A. V. Kabashin, "Phase jumps and interferometric surface plasmon resonance imaging," *Appl. Phys. Lett.* **75**(25), 3917–3919 (1999).
37. V. G. Kravets et al., "Singular phase nano-optics in plasmonic metamaterials for label-free single-molecule detection," *Nat. Mater.* **12**(4), 304–309 (2013).
38. S. M. Hein and H. Giessen, "Retardation-induced phase singularities in coupled plasmonic oscillators," *Phys. Rev. B* **91**(20), 205402 (2015).
39. P. Miao et al., "Orbital angular momentum microlaser," *Science* **353**(6298), 464–467 (2016).
40. Q. Song et al., "Plasmonic topological metasurface by encircling an exceptional point," *Science* **373**(6559), 1133–1137 (2021).
41. G. Ermolaev et al., "Topological phase singularities in atomically thin high-refractive-index materials," *Nat. Commun.* **13**(1), 2049 (2022).
42. F. Yesilkoy et al., "Phase-sensitive plasmonic biosensor using a portable and large field-of-view interferometric microarray imager," *Light Sci. Appl.* **7**(2), 17152 (2018).
43. A. V. Kabashin, V. G. Kravets, and A. N. Grigorenko, "Label-free optical biosensing: going beyond the limits," *Chem. Soc. Rev.* **52**(18), 6554–6585 (2023).
44. R. P. Jenkins, S. D. Campbell, and D. H. Werner, "Establishing exhaustive metasurface robustness against fabrication uncertainties through deep learning," *Nanophotonics* **10**(18), 4497–4509 (2021).
45. E. W. Wang et al., "Robust design of topology-optimized metasurfaces," *Opt. Mater. Express* **9**(2), 469–482 (2019).
46. S. Fan, W. Suh, and J. D. Joannopoulos, "Temporal coupled-mode theory for the Fano resonance in optical resonators," *J. Opt. Soc. Am. A* **20**(3), 569 (2003).
47. Z. Miao et al., "Widely tunable terahertz phase modulation with gate-controlled graphene metasurfaces," *Phys. Rev. X* **5**, 41027 (2015).
48. H. A. Haus, *Waves and Fields in Optoelectronics*, Prentice-Hall, Englewood Cliffs, NJ (1984).
49. J.-H. Park et al., "Symmetry-breaking-induced plasmonic exceptional points and nanoscale sensing," *Nat. Phys.* **16**(4), 462–468 (2020).
50. J.-H. Park et al., "Hybridized metamaterial platform for nanoscale sensing," *Opt. Express* **25**(13), 15590–15598 (2017).

Biographies of the authors are not available.